Toward Synergistic Learning for Liver Vessel and Couinaud Segmentations

Yue Qiu [1,2], Yan Li [1,2], Yuqi Tong [1,2], Qixuan Liu [1,2], Qian Yang [3], Shi Qiu [1,2] (✉), Pheng-Ann Heng [1,2], and Chi-Wing Fu [1,2]

[1] Dept. of Computer Science and Engineering, The Chinese University of Hong Kong
[2] Institute of Medical Intelligence and XR, The Chinese University of Hong Kong
[3] Shanghai Jiao Tong University
{yqiu23, shiqiu}@cse.cuhk.edu.hk

Abstract. Accurate modeling of liver anatomy and its vascular architecture from medical imaging is critical for surgical planning and navigation in liver cancer treatment. Although liver Couinaud segments are fundamentally defined by the branching topology of portal and hepatic veins, current methods typically treat vessel and Couinaud segmentation as isolated tasks, neglecting their intrinsic anatomical dependencies. To bridge this gap, we introduce a vascular skeleton-aware learning framework that jointly addresses both tasks through three key components. First, we propose a multi-branch Tri-directional Convolution (TriDConv) module to explicitly capture anisotropic vascular morphology from CT data along orthogonal spatial axes. Second, we design a Vascular Attention and Spatial-Topology (VAST) mechanism that enforces long-range structural coherence and topological continuity by integrating sequential attention with anatomical geometric constraints. Third, we introduce a novel point-sampling strategy leveraging vascular representations as geometric priors to guide 3D Couinaud segmentation. Extensive evaluations on public datasets demonstrate that our method consistently outperforms state-of-the-art approaches by significant margins across both volumetric and surface distance metrics. Code is available at https://github.com/YueQiu0911/VSA-Liver.

Keywords: Couinaud Segmentation · Vessel Segmentation · Anatomical Consistency · Vascular Topology

1 Introduction

Primary liver cancer (PLC) is the third leading cause of cancer-related deaths worldwide [24], with partial hepatectomy remaining one of the primary curative treatments. Surgeons rely on the precise identification of hepatic vasculature and functional liver segments, estimating liver remnant and developing effective plans for liver resection surgery. Theoretically, the hepatic vascular system determines the liver's perfusion and drainage territories, serving as the anatomical basis for the Couinaud segmentation scheme, which divides the liver into eight functionally independent segments [2]. Therefore, accurate segmentations

of both liver vessels and Couinaud segments are crucial for safe and effective PLC treatment. While clinically indispensable, automating these segmentations via medical image computing presents substantial challenges. Liver vessels exhibit small diameters, complex branching patterns, and high anatomical variability. More importantly, Couinaud segment boundaries are devoid of visible image gradients and must be indirectly deduced from the vascular topology that governs flow territories [1,4]. Despite the fact that Couinaud segments are inherently dictated by the spatial distribution of the hepatic vasculature, existing methods struggle to effectively couple these tasks. Current approaches either address these segmentations as independent tasks, neglecting the anatomical significance of vascular structures [17,12,20], or rely heavily on manually annotated vessel masks [29,5], hindering seamless integration into automated clinical workflows.

In this work, we propose a synergistic learning framework that fundamentally breaks this bottleneck. Rather than relying on costly prerequisite vessel annotations, our model introduces an anatomy-driven paradigm. It first extracts geometrically-aware and topologically-consistent vascular representations from CT images to achieve high fidelity vessel segmentation. Crucially, these explicitly predicted vascular structures are then harnessed as spatial priors to govern the highly ill-posed delineation of Couinaud segments. By rigorously exploiting this underlying anatomical consistency, our approach seamlessly bridges the two tasks and empowers the predicted vasculature to naturally dictate the functional parcellation of the liver. Since Couinaud segments are anatomically determined by vascular topology but not vice versa, our framework propagates vascular priors in a single, anatomically faithful direction rather than through bidirectional co-optimization. This asymmetric design mirrors the liver's anatomical hierarchy, where vascular branching dictates segmental boundaries. To realize this anatomy-guided integration and capture vascular topology, we introduce several tailored components. Unlike conventional 3D isotropic convolutions that operate on symmetric receptive fields but overlook the highly anisotropic and elongated nature of vascular structures, we develop Tri-directional Convolution (TriDConv). By applying a parallel multi-branch design with factorized dimensional filters, TriDConv encodes features along independent spatial directions without imposing heavy computational overhead. These features are then refined through our Vascular Attention and Spatial-Topology (VAST) mechanism, which applies sequential channel–spatial attentions. VAST also incorporates topological modeling of the hepatic vascular system via geometric constraints, further enhancing vessel path connectivity and branching consistency. Furthermore, to translate these optimized features into exact Couinaud segmentations across the volumetric space, we formulate a Skeleton-Aware Sampling (SAS) strategy that captures critical vasculature responses for precise boundary localization. By explicitly predicting vasculature to dictate anatomical parcellation, our method successfully eliminates the restrictive reliance on prior ground-truth vessel masks, significantly alleviating the laborious manual delineation burdens placed on clinical practitioners.

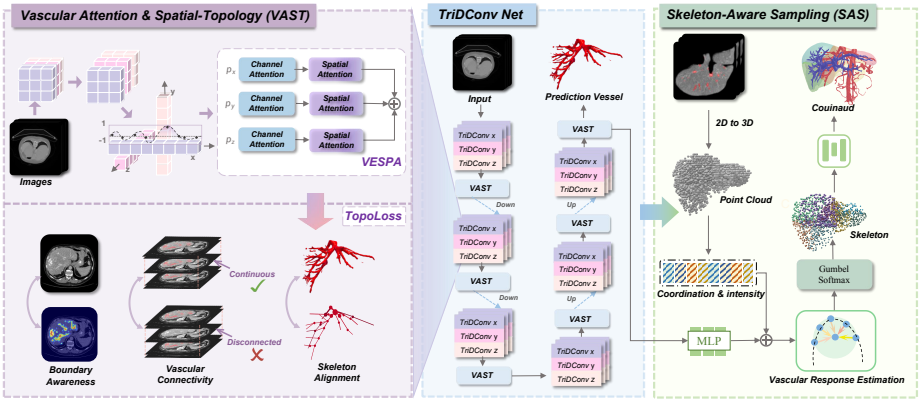

Fig. 1. Overview of the proposed framework. It integrates TriDConv Net for feature extraction, VAST for topological enhancement, and SAS for skeleton-aware Couinaud segmentation.

2 Methodology

Our framework couples liver vessel and Couinaud segmentations by exploiting anatomical correlations (Fig. 1). First, Tri-directional Convolution (TriDConv) extracts multi-resolution anisotropic vessel features, which are refined by the Vascular Attention and Spatial-Topology (VAST) mechanism. These high-fidelity representations then yield precise vessel segmentation while driving Couinaud partitioning via Skeleton-Aware Sampling (SAS).

2.1 Tri-directional Convolution for Local Vascular Feature Extraction

Liver CT data exhibits intricate anatomical structures within its vascular network, geometrically characterized by distinct directional bifurcations, elongated curvatures, and varying thickness. However, these complex geometric features present substantial challenges for regular volumetric CNNs. Standard 3D convolutions rely on isotropic receptive fields, which struggle to isolate continuous vascular paths without simultaneously accumulating noisy background responses from adjacent tissue. To overcome these limitations, we introduce the Tri-directional Convolution (TriDConv), a multi-branch architecture to explicitly model local geometric vessel cues along distinct spatial axes.

Given an intermediate input feature map $\mathbf{X}$, our module computes local representations as:

$$\mathbf{F}_{\text{TriDConv}} = \Psi_{\text{merge}}\Big(\big[\Phi_{\text{iso}}(\mathbf{X});\ \Phi_x(\mathbf{X});\ \Phi_y(\mathbf{X});\ \Phi_z(\mathbf{X})\big]\Big), \tag{1}$$

where $[\cdot;\cdot]$ denotes channel-wise concatenation. Specifically, $\Phi_{\text{iso}}(\cdot)$ serves as an isotropic anchor to preserve essential local context, such as non-directional vascular bifurcations. To explicitly track elongated geometries, the branches $\Phi_x(\cdot)$,

$\Phi_y(\cdot)$, and $\Phi_z(\cdot)$ employ uniaxial anisotropic filters. By strictly restricting operations along the sagittal, coronal, and axial dimensions respectively, this orthogonal decoupling forces the network to trace vascular continuity without enlarging the global parameter space. Following the multi-branch concatenation, a cross-channel projection function $\Psi_{\text{merge}}(\cdot)$ fuses the diverse directional responses into a unified cohesive feature map. Recognizing that directional relevance varies across regions, these representations are subsequently modulated through an enhanced channel-spatial hybrid attention [8]. In summary, TriDConv intrinsically balances computational efficiency and geometrically-motivated anisotropic perception.

2.2 Global Vascular Feature Enhancement with Spatial-Topology

Vascular structures exhibit complex branching geometries, where discontinuities in segmented results cause severe violations of anatomical consistency. To ensure both high-fidelity region recognition and global structural connectivity, we propose the Vascular Attention and Spatial-Topology (VAST) module. Specifically, the Vascular Enhancement Spatial-Profile Attention (VESPA) factorizes the feature tensor into three orthogonal geometric profiles (p_x, p_y, p_z), applying sequential channel-spatial attention [27] to explicitly recalibrate and amplify tubular structures against noisy hepatic backgrounds. Subsequently, to topologically regularize this enhanced feature space, we introduce TopoLoss to bridge voxel intensity alignment with abstract connectivity constraints:

$$\mathcal{L} = \mathcal{L}_{\text{reg}}(\mathbf{P}, \mathbf{G}) + \lambda_b \mathcal{L}_{\text{Bound}} + \lambda_t \mathcal{L}_{\text{Topo}}, \tag{2}$$

where $\mathcal{L}_{\text{reg}}$ integrates standard intensity classification (e.g., BCE or Dice) and volumetric overlap regularization between the prediction $\mathbf{P}$ and the ground truth $\mathbf{G}$, while hyperparameters λ_b and λ_t balance the following structural and geometric penalties. Traditional voxel-wise losses systematically fail to penalize topological errors such as disconnected branches or broken vessel centerlines. Our boundary-aware term $\mathcal{L}_{\text{Bound}} = \mathbb{E}[\|\mathbf{P} - \mathbf{G}\|^2 \cdot \exp(-\mathbf{D}^2/\tau)]$ forces sharp delineation at vascular interfaces by mapping the prediction error into a distance transform field $\mathbf{D}$, where τ concentrates the gradient updates heavily on misaligned structural edges. Crucially, addressing the core limitation of pixel-level classification, the topology-preserving term $\mathcal{L}_{\text{Topo}}$ abstractly models both topological persistence (connectivity count) and morphological coherence (shape skeletonization) into a unified distance geometric space:

$$\mathcal{L}_{\text{Topo}} = \underbrace{\text{EMD}\big(\mathcal{T}(\mathbf{P}), \mathcal{T}(\mathbf{G})\big)}_{\text{Persistence Penalty}} + \underbrace{\left(1 - 2\frac{|\mathcal{S}(\mathbf{P}) \cap \mathcal{S}(\mathbf{G})|}{|\mathcal{S}(\mathbf{P})| + |\mathcal{S}(\mathbf{G})|}\right)}_{\text{Morphological Discrepancy}}, \tag{3}$$

where $\mathcal{T}(\cdot)$ extracts topological features, including connected component cardinality and branch lengths, to construct the Earth Mover's Distance (EMD) [22] metric for penalizing incorrect vascular branching structures. Concurrently, $\mathcal{S}(\cdot)$

Table 1. Quantitative results of liver vessel segmentation on MSD and LiVS datasets.

Methods	MSD Dataset				LiVS Dataset			
	Dice↑	VOE↓	ASSD↓	HD95↓	Dice↑	VOE↓	ASSD↓	HD95↓
U-Net [21]	57.16	56.20	8.15	2.91	72.85	39.82	4.29	17.38
3D U-Net [3]	64.23	52.10	3.22	1.79	79.48	33.70	0.81	4.06
V-Net [18]	66.96	48.87	2.20	1.28	74.23	40.55	1.04	5.33
DCSAU-Net [28]	70.67	44.87	2.27	1.44	78.97	33.36	1.15	5.24
DualNet [13]	67.40	46.53	5.74	2.27	74.81	37.08	2.19	9.84
MSFNet [15]	67.17	48.93	1.99	1.19	74.70	40.14	0.94	4.81
TransFusionNet [25]	55.09	57.45	8.05	2.64	75.79	35.28	2.77	10.97
CaraNet [14]	69.41	46.45	1.75	1.35	72.38	44.36	0.93	4.90
LSFNet [6]	71.07	44.25	2.65	1.88	81.59	30.70	0.92	4.87
Ours	**74.97**	**39.52**	**1.68**	**1.13**	**83.48**	**28.03**	**0.67**	**3.54**

adopts the differentiable 3D morphological skeletonization operator [16] to enforce center-line continuity. By prioritizing this abstract topological divergence, our approach prevents broken vessel segments and strictly ensures anatomical fidelity.

2.3 Skeleton-Aware Sampling for Couinaud Segmentation

Anatomically, the structural topology of the hepatic vascular system serves as the anatomical basis for the functional division of the liver. Specifically, Couinaud segments are entirely delineated by the ramification paths and blood drainage territories of the portal and hepatic veins [2]. Recognizing this physiological correlation, we assert that a key advantage of our synergistic framework lies in explicitly maintaining this anatomical consistency. Consequently, we propose the Skeleton-Aware Sampling (SAS) module, which bridges the two interconnected tasks by translating high-dimensional vascular descriptors into resilient geometric priors, allowing the segmentation network to adaptively focus on topologically critical boundaries. Rather than sampling volumetric coordinates uniformly, SAS learns a dynamic spatial distribution strictly driven by the extracted vessel topology. Given 3D spatial coordinate $\mathbf{p}_i$, its raw intensity $\mathbf{i}_i$, and the corresponding vascular skeleton feature $\mathbf{f}_i^{\text{vessel}}$ optimized from the successive VAST cascade, we first formulate a skeletal-aware proxy descriptor $\mathbf{h}_i$ via non-linear projection. To perceive the surrounding structural context, SAS aggregates geometric cues and global contextual dependencies into a joint representation manifold. From this aggregated context, the abstract skeletal response score s_i for evaluating spatial significance is modeled as

$$s_i = (\mathbf{W}_w \mathbf{h}_i) \cdot \log\Big(1 + \text{Softplus}(\mathbf{W}_r \mathbf{h}_i)\Big), \tag{4}$$

where $\mathbf{W}_w$ and $\mathbf{W}_r$ are learnable projection matrices. To integrate this discrete boundary-seeking policy into an end-to-end continuous optimization process, we

employ the Gumbel-Softmax reparameterization strategy [26]. The probability π_i of selectively sampling the i-th topological point is estimated by:

$$\pi_i = \frac{\exp\left((s_i + g_i)/\tau\right)}{\sum_j \exp\left((s_j + g_j)/\tau\right)}, \quad g_i \sim \text{Gumbel}(0, 1), \tag{5}$$

where g_i introduces structured stochastic perturbation and temperature τ modulates the selection sharpness. This differentiable subset selection guarantees that backpropagation geometrically guides the sampling density explicitly toward vascular forks and flow frontiers. Unlike direct prior injection that simply concatenates vessel masks as an extra input channel, SAS uses the learned skeletal response score to actively bias the sampling density toward vascular bifurcations, precisely the sites where Couinaud boundaries are anatomically defined.

By exclusively prioritizing physiologically skeletal-relevant points, SAS successfully bridges the modalities and enforces strict anatomical boundaries for effective Couinaud partitioning.

3 Experiments

3.1 Experimental Setup

We evaluate our framework on three public datasets: MSD [23] and LiVS [6] for hepatic vessel segmentation, and MSD8 [23] for Couinaud segmentation. We specifically utilize the MSD8 subset as it uniquely provides the requisite 8-segment annotations missing from the broader MSD cohort. All datasets are randomly split into training and testing sets with a ratio of 8:2. All experiments are conducted on two NVIDIA RTX 4090 GPUs using PyTorch. For fair comparisons, we train and test all comparison methods with the same experimental settings and configurations. For the liver vessel segmentation phase, our model is optimized by the Adam optimizer [10] with an initial learning rate of 1×10^{-3}, and trained for 100 epochs with a batch size of 2. For the subsequent Couinaud segmentation task, we freeze the pre-trained TriDConv and VAST modules to extract vascular feature representations. This two-stage design is a deliberate choice grounded in liver anatomy: Couinaud segments are determined by vascular topology but exert no influence on vessel geometry, so a frozen, high-fidelity vascular encoder provides a stable and anatomically faithful prior rather than a target for bidirectional co-adaptation. These skeleton-aware priors are then seamlessly injected into our SAS module, which is jointly trained alongside baseline models following their default architectural configurations.

3.2 Comparison with State-of-the-art Methods

Liver Vessel Segmentation. We evaluate our framework against nine models on the MSD and LiVS datasets. As shown in Tab. 1, our approach consistently outperforms all baselines. Notably, compared to LSFNet [6], we improve the Dice score by 3.90% on MSD and 1.89% on LiVS. Furthermore, our spatial-topology

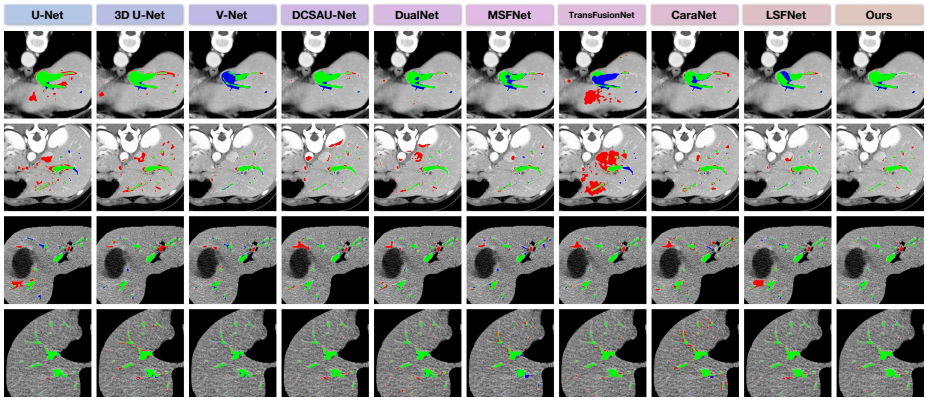

Fig. 2. The qualitative results of liver vessel segmentation on the MSD and LiVS datasets. In the comparisons, green indicates *correct* predictions, red denotes *incorrect* predictions, and blue represents ground truths that were *not predicted*.

Table 2. Quantitative results of Couinaud segmentation on the MSD8 dataset.

Methods	**Dice (%)↑**	**ACC (%)↑**	**ASD↓**
3D UNet [3]	88.78 ± 2.66	79.93 ± 4.27	1.76 ± 1.31
3D UXNet [11]	88.40 ± 3.64	79.40 ± 5.81	1.91 ± 3.31
SwinUNetR [7]	80.45 ± 5.03	67.58 ± 6.96	2.52 ± 1.78
BA-DAGNet [9]	86.44 ± 4.05	76.34 ± 6.11	1.89 ± 2.83
PointNet2Plus [19]	82.68 ± 7.36	70.80 ± 5.27	7.33 ± 4.52
PointNet2Plus + **Ours**	**85.05 ± 5.22**	**74.33 ± 7.58**	**4.53 ± 2.90**
ASG-PVN [29]	89.72 ± 4.77	81.67 ± 7.37	5.49 ± 6.03
ASG-PVN + **Ours**	**92.43 ± 2.29**	**86.00 ± 3.90**	**1.46 ± 0.83**

guidance significantly reduces surface errors, dropping HD95 from 1.88 mm to 1.13 mm on MSD and 4.87 mm to 3.54 mm on LiVS. Qualitatively (Fig. 2), competing methods like TransFusionNet [25] struggle with severe false positives and missed capillaries. Conversely, our method faithfully isolates intricate distal vascular paths without accumulating noisy background responses, aligning with the ground truth.

Couinaud Liver Segmentation. To evaluate skeleton-guided adaptability, we benchmark against top-performing voxel and point-based architectures (Tab. 2). The integration of our SAS module with ASG-PVN achieves the highest Dice (92.43%) and lowest Average Surface Distance (1.46 mm). While standalone voxel methods exhibit competitive volume overlap, they lack geometric boundary precision. As illustrated in the zoomed-in regions of Fig. 3, the standalone baseline produces segment misclassifications and jagged inter-segment boundaries. In contrast, the green bounding boxes reveal that our SAS module successfully removes these scattered, incorrect voxel predictions along the boundary

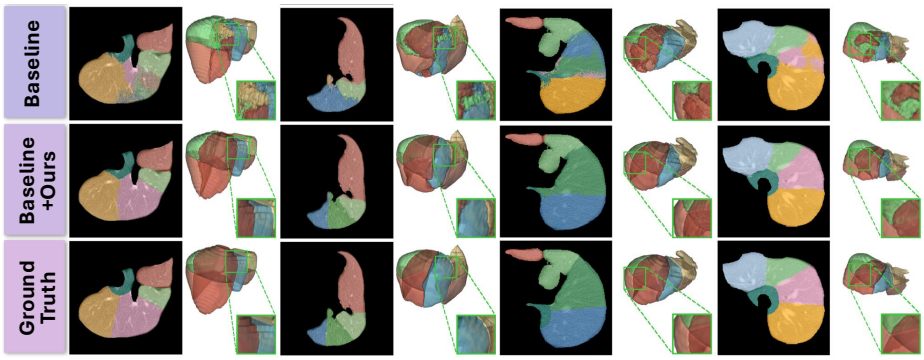

Fig. 3. The qualitative results of liver Couinaud segmentation on the MSD8 dataset. In the comparisons, we use different colors to denote eight Couinaud segments.

lines. This dramatically smooths the topological artifacts, yielding inter-segment demarcations that inherently respect the underlying vascular flow territories.

Table 3. Ablation study of the VESPA module and $\mathcal{L}_{\text{Topo}}$ constraint for liver vessel segmentation on the MSD and LiVS datasets.

VESPA	$\mathcal{L}_{\text{Topo}}$	MSD Dataset				LiVS Dataset			
		Dice↑	VOE↓	ASSD↓	HD95↓	Dice↑	VOE↓	ASSD↓	HD95↓
		73.12	41.81	2.89	2.17	82.78	29.11	0.74	3.89
✓		73.85	40.79	2.67	1.83	83.46	28.11	0.68	3.84
	✓	74.43	40.14	2.22	1.24	83.01	28.67	0.73	3.70
✓	✓	**74.97**	**39.52**	**1.68**	**1.13**	**83.48**	**28.03**	**0.67**	**3.54**

3.3 Ablation Study

To evaluate the effects of the VESPA module and TopoLoss constraints, we perform an ablation study of liver vessel segmentation, as shown in Tab. 3. The model using only the baseline achieves the lowest performance, highlighting the need for both local vascular feature refinement and global structural constraints. After adding VESPA, we obtain notable improvements, increasing the Dice score by +0.73% and reducing ASSD from 2.89 to 2.67. When both VESPA and TopoLoss are combined, the model achieves the best overall performance, with a Dice score of 74.97%, the lowest VOE (39.52%), as well as improvements in both ASSD and HD95 metrics. These results show that the combination of VESPA and TopoLoss leads to enhanced vessel anatomy predictions.

4 Conclusion

In this work, we present a vascular feature-driven framework that synergistically learns liver vessel and Couinaud segmentations. Using both 2D and 3D medical data, our framework consists of TriDConv, VAST, SAS modules, enhancing anatomical consistency for accurate liver vessel and Couinaud segmentations. By effectively modeling the intricate geometry of liver vessels, our framework enables more precise delineation of both vascular structures and Couinaud segments. More importantly, we demonstrate that the synergy between liver vessel and Couinaud segmentations ensures reliable and clinically meaningful context, supporting future integration into real-world surgical planning and guidance workflows. Since current framework has not been explicitly evaluated under pathological variations, e.g., tumors distorting normal liver anatomy, our future work will focus on enhancing domain generalization abilities and pathological robustness.

Acknowledgments. The work described in this paper was supported by the Research Grants Council of the Hong Kong Special Administrative Region, China, under Project T45-401/22-N; and in part by The Chinese University of Hong Kong, under Project 4055299.

Disclosure of Interests. The authors have no competing interests to declare that are relevant to the content of this article.

References

1. Bell-Allen, N., Mastrocostas, K., Roseverne, L., Samra, J., Brown, K.: Three-dimensional reconstruction of hepatic imaging to tailor complex liver resection: A preliminary australian single centre experience. ANZ Journal of Surgery (2025)
2. Chen, Y., Yue, X., Zhong, C., Wang, G.: Functional region annotation of liver ct image based on vascular tree. BioMed research international **2016**(1), 5428737 (2016)
3. Çiçek, Ö., Abdulkadir, A., Lienkamp, S.S., Brox, T., Ronneberger, O.: 3d u-net: learning dense volumetric segmentation from sparse annotation. In: International conference on medical image computing and computer-assisted intervention. pp. 424–432. Springer (2016)
4. Cotsoglou, C., Granieri, S., Bassetto, S., Bagnardi, V., Pugliese, R., Grazi, G.L., Guglielmi, A., Ruzzenente, A., Aldrighetti, L., Ratti, F., et al.: Dynamic surgical anatomy using 3d reconstruction technology in complex hepato-biliary surgery with vascular involvement. results from an international multicentric survey. HPB **26**(1), 83–90 (2024)
5. Fan, W., Fang, H., Li, R., Lin, Y., An, C., Luo, X.: Anatomy-aware frequency-attention transformer networks for liver couinaud ct/mr segmentation. In: International Conference on Medical Image Computing and Computer-Assisted Intervention. pp. 55–65. Springer (2025)
6. Gao, Z., Zong, Q., Wang, Y., Yan, Y., Wang, Y., Zhu, N., Zhang, J., Wang, Y., Zhao, L.: Laplacian salience-gated feature pyramid network for accurate liver vessel segmentation. IEEE Transactions on Medical Imaging **42**(10), 3059–3068 (2023)

7. Hatamizadeh, A., Nath, V., Tang, Y., Yang, D., Roth, H.R., Xu, D.: Swin unetr: Swin transformers for semantic segmentation of brain tumors in mri images. In: International MICCAI brainlesion workshop. pp. 272–284. Springer (2021)
8. Hu, J., Shen, L., Sun, G.: Squeeze-and-excitation networks. In: Proceedings of the IEEE conference on computer vision and pattern recognition. pp. 7132–7141 (2018)
9. Jia, X., Qian, C., Yang, Z., Xu, H., Han, X., Ren, H., Wu, X., Ma, B., Yang, D., Min, H.: Boundary-aware dual attention guided liver segment segmentation model. KSII Transactions on Internet & Information Systems **16**(1), 16 (2022)
10. Kingma, D.P., Ba, J.: Adam: A method for stochastic optimization. arXiv preprint arXiv:1412.6980 (2014)
11. Lee, H.H., Bao, S., Huo, Y., Landman, B.A.: 3d ux-net: A large kernel volumetric convnet modernizing hierarchical transformer for medical image segmentation. arXiv preprint arXiv:2209.15076 (2022)
12. Li, Y., Li, R., Qiu, Y., Liu, Q., Pei, J., Qiu, S., Heng, P.A.: Sspt: Spiking serialized point transformer for couinaud segmentation in 3d medical data. In: International Conference on Medical Image Computing and Computer-Assisted Intervention. Springer (2026)
13. Liu, Q., Liu, H., Zhao, Y., Liang, Y.: Dual-branch network with dual-sampling modulated dice loss for hard exudate segmentation in color fundus images. IEEE Journal of Biomedical and Health Informatics **26**(3), 1091–1102 (2021)
14. Lou, A., Guan, S., Ko, H., Loew, M.H.: Caranet: context axial reverse attention network for segmentation of small medical objects. In: Medical Imaging 2022: Image Processing. vol. 12032, pp. 81–92. SPIE (2022)
15. Ma, X., Zhang, X., Pun, M.O., Liu, M.: Msfnet: multi-stage fusion network for semantic segmentation of fine-resolution remote sensing data. In: IGARSS 2022-2022 IEEE International Geoscience and Remote Sensing Symposium. pp. 2833–2836. IEEE (2022)
16. Menten, M.J., Paetzold, J.C., Zimmer, V.A., Shit, S., Ezhov, I., Holland, R., Probst, M., Schnabel, J.A., Rueckert, D.: A skeletonization algorithm for gradient-based optimization. In: Proceedings of the IEEE/CVF International Conference on Computer Vision. pp. 21394–21403 (2023)
17. Miao, D., Zhao, Y., Ren, X., Dou, M., Yao, Y., Xu, Y., Cui, Y., Liu, A.: A multi-task based deep learning framework with landmark detection for mri couinaud segmentation. IEEE Journal of Translational Engineering in Health and Medicine **12**, 697–710 (2024)
18. Milletari, F., Navab, N., Ahmadi, S.A.: V-net: Fully convolutional neural networks for volumetric medical image segmentation. In: 2016 fourth international conference on 3D vision (3DV). pp. 565–571. Ieee (2016)
19. Qi, C.R., Yi, L., Su, H., Guibas, L.J.: Pointnet++: Deep hierarchical feature learning on point sets in a metric space. Advances in neural information processing systems **30** (2017)
20. Qiu, L., Chi, W., Xing, X., Rajendran, P., Li, M., Jiang, Y., Pastor-Serrano, O., Yang, S., Ji, Y., Wen, Q.: Artificial intelligence-enhanced couinaud segmentation for precision liver cancer therapy. Biomedical Signal Processing and Control **120**, 110100 (2026)
21. Ronneberger, O., Fischer, P., Brox, T.: U-net: Convolutional networks for biomedical image segmentation. In: International Conference on Medical image computing and computer-assisted intervention. pp. 234–241. Springer (2015)
22. Rubner, Y., Tomasi, C., Guibas, L.J.: The earth mover's distance as a metric for image retrieval. International journal of computer vision **40**(2), 99–121 (2000)

23. Simpson, A.L., Antonelli, M., Bakas, S., Bilello, M., Farahani, K., Van Ginneken, B., Kopp-Schneider, A., Landman, B.A., Litjens, G., Menze, B., et al.: A large annotated medical image dataset for the development and evaluation of segmentation algorithms. arXiv preprint arXiv:1902.09063 (2019)
24. Sung, H., Ferlay, J., Siegel, R.L., Laversanne, M., Soerjomataram, I., Jemal, A., Bray, F.: Global cancer statistics 2020: Globocan estimates of incidence and mortality worldwide for 36 cancers in 185 countries. CA: a cancer journal for clinicians **71**(3), 209–249 (2021)
25. Wang, X., Zhang, X., Wang, G., Zhang, Y., Shi, X., Dai, H., Liu, M., Wang, Z., Meng, X.: Transfusionnet: Semantic and spatial features fusion framework for liver tumor and vessel segmentation under jetsontx2. IEEE Journal of Biomedical and Health Informatics **27**(3), 1173–1184 (2022)
26. Wen, C., Yu, B., Tao, D.: Learnable skeleton-aware 3d point cloud sampling. In: Proceedings of the IEEE/CVF Conference on Computer Vision and Pattern Recognition. pp. 17671–17681 (2023)
27. Woo, S., Park, J., Lee, J.Y., Kweon, I.S.: Cbam: Convolutional block attention module. In: Proceedings of the European conference on computer vision (ECCV). pp. 3–19 (2018)
28. Xu, Q., Ma, Z., Duan, W., et al.: Dcsau-net: A deeper and more compact split-attention u-net for medical image segmentation. Computers in biology and medicine **154**, 106626 (2023)
29. Zhang, X., Ali, S., Liu, T., Zhao, X., Cui, Z., Han, M., Ma, S., Zhu, J., Kang, Y., Wang, L., et al.: Robust and smooth couinaud segmentation via anatomical structure-guided point-voxel network. Computers in Biology and Medicine **182**, 109202 (2024)